# Convective Assembly of Antireflective Silica Coatings with Controlled Thickness and Refractive Index

Brian G. Prevo,[†] Yeon Hwang,[‡] and Orlin D. Velev*[,†]

*Department of Chemical and Biomolecular Engineering, North Carolina State University, Raleigh, North Carolina 27695-7905, and Department of Materials Science and Engineering, Seoul National University of Technology, Seoul 139-743, Korea*

*Received February 23, 2005. Revised Manuscript Received April 9, 2005*

Convective assembly at high volume fraction was used to deposit silica nanoparticle coatings onto glass and silicon substrates. By allowing control of the film structure and thickness, this technique provides a means for making large-scale coatings with antireflective properties. The reflectance was reduced by 50% for silicon (at 600 nm) and by 70% for single glass/air surface. Microstructural investigations using SEM, AFM, profilometry, and ellipsometry provided good correlation to the observed macroscopic optical properties. By virtue of the coatings' uniformity, the reflectance and transmission spectra from both substrates could be modeled well by classical reflection relations, using a volume-averaged refractive index. Data analysis showed that the relatively high packing fraction in nanocoatings made from monodisperse spheres is responsible for the limit on antireflective capabilities. To overcome this restriction, low-density silica coatings were made from binary colloidal mixtures of different diameter $SiO_2$ particles. The packing fraction of these coatings was further optimized to yield 88% maximal reduction in the reflectance of glass surfaces. The technique is simple, inexpensive, and scalable.

## Introduction

Antireflective coatings on glass substrates were first discovered in 1817 by Fraunhofer, and a few years later, Poisson and Fresnel defined the phenomenon as destructive interference between the light reflected from a substrate and the light reflected from a thin film coating that substrate.[1] Today, thin film technologies comprise a multibillion dollar industry, and coatings (or multiple coating stacks) for improved light transmission (or reduced reflectance) provide benefits to a wide variety of technological applications from optical filters and photovoltaics (solar cells, photodetectors) to windows, eye-wear, display screens, and myriad other materials.[1,2]

An ideal homogeneous antireflective (AR) coating achieves effectively 0% reflection at a specific wavelength when its refractive index, $n_c$, meets the condition of $n_c = (n_a n_s)^{1/2}$, where $n_a$ and $n_s$ are the refractive indices of the air and the substrate, respectively.[3] A glass substrate ($n_s = 1.52$) requires $n_c = 1.23$. Natural or synthetic materials having such low refractive indexes are either rare and expensive to obtain or synthesize or difficult to manipulate in thin film form.[4] However, porous or microscopically layered dielectric materials can easily achieve an effective volume-averaged refractive index approaching 1.23, provided that the pore size is much smaller than the electromagnetic wavelengths of interest. The AR materials applications listed above require deposition of coatings on a wide variety of substrates, and the optimal $n_c$ required by these substrates can be adjusted by tuning the degree of porosity in the coating.

There are a variety of top-down and bottom-up techniques for making thin coatings with tunable porosity. One approach, used by Fraunhofer himself,[1] is to roughen the substrate by leaching out material from its surface via chemical etching to produce small pores; similar processes are presently used in solar cells.[5−7] The main disadvantages of chemical etching are the length of etching time required and the use of highly hazardous acid etchants such as HF or $H_2SiF_6{\cdot}SiF_4$. Improvements in a vacuum diffusion pumps and laser technologies have made laser ablation a popular, albeit expensive, alternative route for etching of a substrate to create a roughened, porous surface layer.[8] Rather than etching, porous layers can also be produced by depositing particulate materials onto the substrate. Sputtering can be used to deposit thin layers on many kinds of substrates.[9] It is a well-developed process for deposition of AR coatings on thermochromic windows,[10−12] display devices such as CRTs,[1]

* Corresponding author. E-mail: odvelev@unity.ncsu.edu.
[†] North Carolina State University.
[‡] Seoul National University of Technology.

(1) Macleod, H. A. *Thin Film Optical Filters*, 2nd ed.; Adam Hilger Ltd.: Bristol, U.K., 1986.
(2) Martinu, L.; Poltras, D. *J. Vac. Sci. Technol., A* **2000**, *18*, 2619−2645.
(3) Fowles, G. R. *Introduction to Modern Optics*, 2nd ed.; Dover Publications: New York, 1989.
(4) Hattori, H. *Adv. Mater.* **2001**, *13*, 51−54.
(5) Schirone, L.; Sotgiu, G.; Califano, F. P. *Thin Solid Films* **1997**, *297*, 296−298.
(6) Vitanov, P.; Kamenova, M.; Tyutyundzhiev, N.; Delibasheva, M.; Goranova, E.; Peneva, M. *Thin Solid Films* **1997**, *297*, 299−303.
(7) Adamian, Z. N.; Hakhoyan, A. P.; Aroutiounian, V. M.; Barseghian, R. S.; Touryan, K. *Sol. Energy Mater. Sol. Cells* **2000**, *64*, 347−351.
(8) Ashfold, M. N. R.; Claeyssens, F.; Fuge, G. M.; Henley, S. J. *Chem. Soc. Rev.* **2004**, *33*, 23−31.
(9) Szczyrbowski, J.; Brauer, G.; Teschner, G.; Zmelty, A. *J. Non-Cryst. Solids* **1997**, *218*, 25−29.
(10) Lee, M. H. *Sol. Energy Mater. Sol. Cells* **2002**, *71*, 537−540.
(11) Jin, P.; Xu, G.; Tazawa, M.; Yoshimura, K. *Jpn. J. Appl. Phys., Part 2* **2002**, *41*, L278−L280.

10.1021/cm050416h CCC: $30.25 
Published on Web 06/04/2005

and a variety of other substrates including plastics.[13,14] Sputtering requires only moderate vacuum for deposition, and a variety of transparent dielectrics such as inorganic oxides ($SiO_2$, $TiO_2$, $Al_2O_3$, and ITO) or $MgF_2$ are commonly used. Physical vapor deposition (PVD) can also be used, and the angle of deposition can be varied to make graded index materials, but the scratch resistance of these coatings is relatively poor.[15] Alternatively, plasma-enhanced chemical vapor deposition (PECVD) can be used to selectively build up coatings on substrates.[2,16] Here the coating quality can be specifically tuned to make even graded layers, but the downsides are use of costly metal−ogranic precursors and high vacuum required for deposition.

Self-assembled AR materials have shown promise from the bottom-up perspective. Phase-separated block copolymer or polymer blend films cast on the substrate can be solvent etched to leave behind a microscopically porous film, which can have good AR properties.[17] Silica sol−gel layers produced via spin-coating or dip-coating processes have been intensively investigated since the late 1970s[18−20] and are currently implemented in AR film production.[21−25] Porous silica sol−gel coatings can potentially be made from self-assembled "inverse opals".[26] Monolayers of silica microspheres were found to substantially reduce the reflectance of bare glass substrate.[27] Electrostatic layer by layer (LBL) deposition of oppositely charged polyelectrolytes[28] and silica particles with polyelectrolytes[4,29] have demonstrated consistent and tunable AR behavior. AR coatings have also been made using soft lithography stamping of oppositely charged colloidal microspheres and polyelectrolytes.[30]

From the standpoint of practical applicability, rapid, simple, scalable, and controlled deposition, coupled with minimal substrate preparation, is desired. Satisfying all these requirements is still a challenge for the present self-assembly methods. We report here a technique for single step deposition of AR silica nanocoatings by controlled convective assembly that requires no substrate pretreatment and no chemical agents and takes place at ambient laboratory conditions. This is a proven technique for rapidly depositing colloidal coatings from nanoparticles to microparticles.[31,32] Uniform coatings of several square centimeters in size can be obtained in minutes from only 10−30 $\mu$L of silica microsphere suspension. We demonstrate AR coatings with tunable microstructure on both glass and silicon substrates and show how the AR behavior can be optimized by deposition of particle mixtures.

## Theoretical Background

Convective assembly is governed by solvent evaporation from a thin liquid film wetting a substrate. A replacement solvent flux from the bulk suspension pulls dispersed particles to the drying region (on the substrate).[33] A simple volumetric flux balance on the drying region shows that the rate of particle assembly in the coating depends on the particle concentration (or volume fraction) in the original suspension, $\phi_p$, a lumped parameter, $K$, which incorporates the rate of solvent evaporation, and the size of the particles.[32] In our technique, the coating thickness, $l$, can be related to the deposition speed, $v_w$, by the following formula based on volumetric balance:

$$l = \frac{K\phi_p}{v_w(1-\epsilon)(1-\phi_p)} \tag{1}$$

Here $\epsilon$ is the fraction of void space in the coating. The void space, $\epsilon$, for thin quasi 2-D coatings of particles is dependent on the number of particle layers and, thus, depends on $l$.[34] In this study, the volume fractions of the suspensions used for coatings were maintained at about 2.5%, and relative humidity was remained at an average of 55%. Thus, the main control parameter was $v_w$, which was used to adjust the thickness and the porosity of the silica nanocoatings.

Here, we briefly review the basic theory behind AR coatings used to interpret our results. The Fresnel coefficient of reflection, $r$, for a thin film coating (of thickness $l$ and refractive index $n_c$) on a semiinfinite transparent slab substrate ($n_s$) is given as follows:[3]

$$r = \frac{n_c(n_a - n_s)\cos kl - i(n_s - n_c^2)\sin kl}{n_c(n_a + n_s)\cos kl - i(n_s + n_c^2)\sin kl} \tag{2}$$

Here the ambient medium is usually air, $n_a = 1$, $k$ is the reciprocal space wavenumber, $k = 2\pi n_c/\lambda$, and $\lambda$ is the wavelength of light. The actual reflectance, $R$, of the coating/substrate system is equal to $|r|^2$. If, however, the thickness

(12) Jin, P.; Xu, G.; Tazawa, M.; Yoshimura, K. *Appl. Phys. A* **2003**, *77*, 455−459.
(13) Lee, J. H.; Cho, J. S.; Koh, S. K.; Kim, D. *Thin Solid Films* **2004**, *449*, 147−151.
(14) Kim, J. Y.; Han, Y. K.; Kim, E. R.; Suh, K. S. *Curr. Appl. Phys.* **2002**, *2*, 123−127.
(15) Kennedy, S. R.; Brett, M. J. *Appl. Opt.* **2003**, *42*, 4573−4579.
(16) Wang, Y. J.; Cheng, X. L.; Lin, Z. L.; Zhang, C. S.; Zhang, F. *Vacuum* **2003**, *72*, 345−349.
(17) Walheim, S.; Schaffer, E.; Mlynek, J.; Steiner, U. *Science* **1999**, *283*, 520−522.
(18) Cathro, K.; Constable, D.; Solaga, T. *Sol. Energy* **1984**, *32*, 573−579.
(19) Yoldas, B. E. *Am. Ceram. Soc. Bull.* **1975**, *54*, 286−288.
(20) Yoldas, B. E. *Appl. Opt.* **1980**, *19*, 1425−1429.
(21) Uhlmann, D. R.; Suratwala, T.; Davidson, K.; Boulton, J. M.; Teowee, G. *J. Non-Cryst. Solids* **1997**, *218*, 113−122.
(22) Zhang, Q. Y.; Wang, J.; Wu, G.; Shen, J.; Buddhudu, S. *Mater. Chem. Phys.* **2001**, *72*, 56−59.
(23) Nostell, P.; Roos, A.; Karlsson, B. *Thin Solid Films* **1999**, *351*, 170−175.
(24) Gombert, A.; Glaubitt, W.; Rose, K.; Dreibholz, J.; Zanke, C.; Blasi, B.; Heinzel, A.; Horbelt, W.; Sporn, D.; Doll, W.; Wittwer, V.; Luther, J. *Sol. Energy* **1998**, *62*, 177−188.
(25) Biswas, P. K.; Devi, P. S.; Chakraborty, P. K.; Chatterjee, A.; Ganguli, D.; Kamath, M. P.; Joshi, A. S. *J. Mater. Sci. Lett.* **2003**, *22*, 181−183.
(26) Velev, O. D.; Jede, T. A.; Lobo, R. F.; Lenhoff, A. M. *Nature* **1997**, *389*, 447−448.
(27) Dimitrov, A. S.; Miwa, T.; Nagayama, K. *Langmuir* **1999**, *15*, 5257−5264.
(28) Hiller, J.; Mendelsohn, J. D.; Rubner, M. F. *Nat. Mater.* **2002**, *1*, 59−63.
(29) Rouse, J. H.; Ferguson, G. S. *J. Am. Chem. Soc.* **2003**, *125*, 15529−15536.
(30) Koo, H. Y.; Yi, D. K.; Yoo, S. J.; Kim, D. Y. *Adv. Mater.* **2004**, *16*, 274−277.
(31) Prevo, B. G.; Fuller, J. C.; Velev, O. D. *Chem. Mater.* **2005**, *17*, 28−35.
(32) Prevo, B. G.; Velev, O. D. *Langmuir* **2004**, *20*, 2099−2107.
(33) Dimitrov, A. S.; Nagayama, K. *Chem. Phys. Lett.* **1995**, *243*, 462−468.
(34) Pansu, B., Pieranski, Pi., Pieranski, Pa. *J. Phys. (Paris)* **1984**, *45*, 331−339.

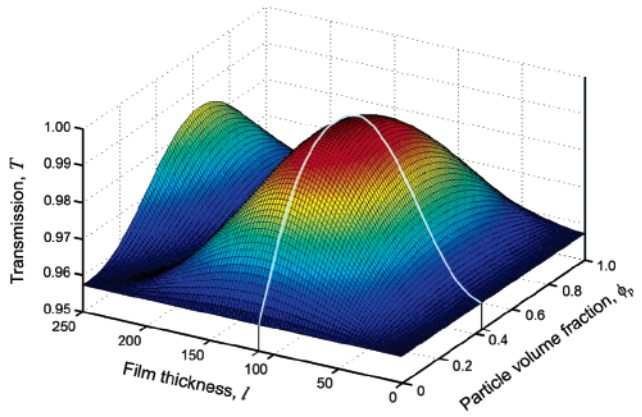


**Figure 1.** Transmission, $T$, calculated for a single-side nonscattering coating on glass using eq 2. The calculation was for a wavelength of 555 nm, where $n_s = 1.52$, $n_a = 1.0$, and the coating refractive index was calculated using eq 4. The optimal $l$ and $\phi_p$ are indicated by highlighted curves.

of the coating is equivalent to a quarter wavelength of the incident light, i.e., $kl = \pi/2$, then the light reflected from the surface of the substrate and from the surface of the coating destructively interfere with each other to achieve zero reflectance, or complete transmission. The reflectance, $R$, for a "quarter wave" coating of such thickness ($l_{1/4} = 0.25\lambda/n_c$) simplifies to

$$R = |r^2| = \frac{(n_s - n_c^2)^2}{(n_s + n_c^2)^2} \qquad (3)$$

and as mentioned earlier, for $R = 0$, $n_c = n_s^{1/2}$. If the coating is a composite made of two or more materials dispersed in subwavelength domains, such as a porous thin film of particles tens of nanometers in diameter, the effective refractive index of the coating, $n_{eff}$, can be estimated by a volume average as follows:

$$n_c = n_{eff} = (\phi_p n_p^2 + (1 - \phi_p) n_a^2)^{1/2}, \qquad \frac{d_p}{\lambda} \ll 1 \qquad (4)$$

Here $\phi_p$ is the volume fraction of the particles in the coating, while $n_p$ and $n_a$ are the refractive indexes of the particles and the ambient medium (air in this case), respectively. The restriction on the maximal particle diameter ($d_p$) is to prevent transmission losses due to scattering. In eq 4, $n_c$ increases monotonically as a function of $\phi_p$ from 1.0 ($n_a$) to 1.46 ($n_p$), an established value for the refractive index of silica particles.[35,36] Due to conservation of energy, $R + A + T = 1$, where $A$ and $T$ are the absorption and transmittance of the system, respectively. Thus, from eqs 2 and 4, the transmittance, $T$, as a function of both $\phi_p$ and $l$ can be calculated as shown in Figure 1. For a representative wavelength of 555 nm (the best resolved color and most readily distinguished wavelength perceived by human eyes[37]), the optimal conditions for maximal transmission through a glass substrate occur at $l \sim 112$ nm and $\phi_p \sim 0.45$, which corresponds to $n_c = 1.23$ (Figure 1). Shorter wavelengths require smaller "quarter wavelength" thicknesses ($l_{1/4}$), and vice versa (e.g., $l_{1/4} \sim 81$ nm for $\lambda = 400$ nm and $l_{1/4} \sim 142$ nm for $\lambda = 700$ nm). Note that the inherent reflective loss for a single glass/air interface is 4.3%, corresponding to a transmission of 95.7%. A glass plate with two parallel surfaces in air (e.g., a microscope slide) would accrue twice this reflective loss, or $R = 8.6\%$, for normally incident light.

## Experimental Section

**Materials.** Silica nanocoatings were made using dispersions of silica nanoparticles of 74 ± 14 nm in diameter (5.67% solids), 134 ± 25 nm (5.42% solids), and mixtures of both. Binary suspensions of various volume fractions of 74 nm silica and 64 ± 12 nm sulfate-stabilized polystyrene nanoparticles (2.6% solids) were also deposited in the mixed particle coating experiments. All particles were obtained from Polysciences, Inc. (PA). The particles sizes were measured using a Zetasizer (Malvern Instruments, U.K.).

**Methods.** Our implementation of the convective assembly process used to deposit the coatings is described in detail in an earlier publication.[32] In brief, ≈30 μL of silica colloid suspension was injected into the wedge formed between two inclined (~23°) surfaces and was entrapped there by capillarity. The liquid meniscus was withdrawn horizontally across the substrate by translating the upper surface at a controlled rate, $v_w$, ranging from 5 to 40 μm/s. Coatings were deposited at ambient conditions in the laboratory: 22 ± 3 °C and 50−60% RH. As the silica sols aged, the deposition speed required for a given coating decreased due to minor increases in particle size. The substrates, either glass microscope slides (frosted, Fisher Scientific, PA) or silicon wafer chips (Silicon Valley Microelectronics, Inc., Santa Clara, CA), were cleaned by immersion in a Nochromix solution (Godax Labs, Inc., Cabin John, MD) for a minimum of several hours followed by complete rinsing with DI water and drying at 70 °C.

Two methods were used to remove the polystyrene (PS) filler particles used in the mixed PS/$SiO_2$ coating experiments. Solvent etching was done by immersing the coated substrate in chloroform (Aldrich, Milwaukee, WI) for 10−15 min and then removing the substrate and rinsing with pure solvent. The coating was then air-dried in a fume hood. Thermal oxidation or pyrolytic etching was performed by heating the samples in a Thermolyne FB 1300 muffle furnace (Barnstead International, IA) to 200 °C for 1 h and then ramping the temperature up in 5 min to 450 °C and holding that temperature for a duration of 0−60 min.

**Coating Characterization.** Coating transmittance and reflectance of normally incident light was measured using a UV/vis spectrophotometer (Jasco V550, Jaso Corp., Japan) over the spectral range of 350−850 nm. A custom sample holder was used. An integrating sphere attachment was used for reflectance mode operation.

The coating thickness on the glass substrates was measured by profilometry (Alpha Step 500, Tencor Instruments, CA). Small regions of the coatings were scratched off down to the bare substrate to facilitate measuring of the film thickness in the uniform central regions of the films. For the silicon substrates, variable angle spectroscopic ellipsometry (VASE, J. A. Woollam Co., Inc.) was used to characterize the film thickness and porosity. The angle of incidence was fixed at 70° (from the normal), and the spectral range probed was 350−850 nm. A multilayer model of air, composite film (air + $SiO_2$), native $SiO_2$ layer, and silicon substrate was used to fit the $\psi-\Delta$ data using the VASE software (J. A. Woollam Co.) by minimizing the mean-squared error. The native oxide layer was measured to be 23 Å. An effective media approximation using both the Maxwell−Garnett or Bruggeman relations for comparison was

(35) Chabanov, A. A.; Jun, Y.; Norris, D. J. *Appl. Phys. Lett.* **2004**, *84*, 3573−3575.
(36) Iler, R. K. *The chemistry of silica*; John Wiley and Sons: New York, 1979.
(37) Nemcsics, A. *Colour dynamics: environmental colour design*; Ellis Harwood: London, 1993.

used for the refractive index (both gave comparable results) of the composite silica coatings, so that the entire model had two fitting parameters: the constituent particle volume fraction, $\phi_p$, and the coating thickness, $l$.

The microstructure of the coatings was studied with a field-emission scanning electron microscope (JEOL, F6400 operating at 4−5 kV) using both top-down and cross-sectional secondary electron imaging. For cross-sectional imaging, the samples were fractured in the direction of deposition along the centerline of the coated substrate. In all cases, a sputtered gold coating of ∼30−60 Å was used to improve sample conductivity.

## Results and Discussion

The optical properties, thickness, and structure of coatings deposited from aqueous silica nanoparticles were characterized in detail. The reproducible deposition by convective assembly requires distinguishing the means for systematic control over coating thickness and refractive index (coating porosity) for a given substrate. Both silicon and glass substrates were used, and several different particle systems were studied in an effort find to the optimal deposition conditions for antireflective behavior.

**Controlling Coating Thickness.** *Silicon Substrates.* The smooth surface of silicon wafers allows obtaining additional microstructural information by methods such as ellipsometry and cross-sectional SEM measurements. These data are difficult to obtain for coatings on glass substrates, because of multiple reflections from the sample during ellipsometry, and strong electrostatic charging effects in the instrument during SEM. The initial hypothesis was that the native oxide layer on the silicon wafer chips would make silicon substrates behave similarly to glass substrates during the deposition process.

Convective assembly offers fine control over the coating properties, but the process requires that the particles deposited should have sufficient time to reach the drying site prior to liquid film rupture.[31,32] Equation 1 predicts that the coating thickness should scale inversely with deposition speed, $l \sim 1/v_w$. Thick coatings require longer deposition time because they comprise more particles/unit coating area. Cross-sectional SEM micrographs of silica nanoparticle coatings deposited at different meniscus withdrawal rates are shown in Figure 2. The coatings exhibited decreasing thickness with increasing deposition speed (all other conditions being held constant). Uniform coverage was observed until deposition speeds exceeded 24 $\mu$m/s. Submonolayers with uniformly distributed voids formed at higher speeds. The thickness measured from the fracture SEM images is plotted as a function of deposition speed, $v_w$, in Figure 3.

The same samples on silicon were characterized by ellipsometry. Film thickness and particle packing fraction data consistent with the SEM findings were obtained, even at submonolayer coverages, where the measured thicknesses approached 70 nm, the approximate single particle diameter (Figure 3). The film thickness data were fitted to the dependence of $\alpha/v_w$, predicted by eq 1, where $\alpha$ is the constant of proportionality. Ellipsometry also showed an increasing porosity approaching 50% for high $v_w$, in good agreement with the SEM observations showing voids distributed throughout the submonolayer coatings at high deposition speeds.

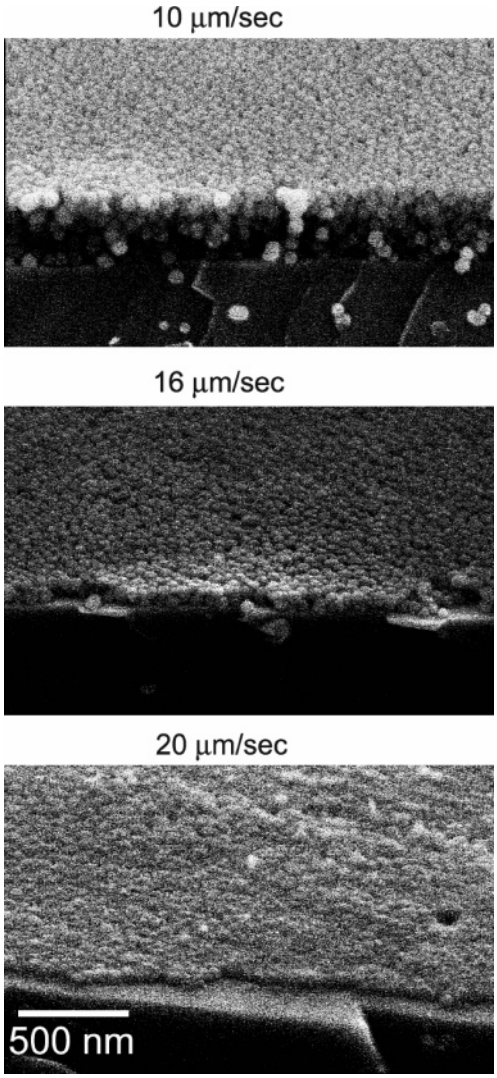


**Figure 2.** Cross-sectional SEM micrographs of coatings from 74 nm silica spheres deposited at various deposition speeds on silicon wafer substrates.

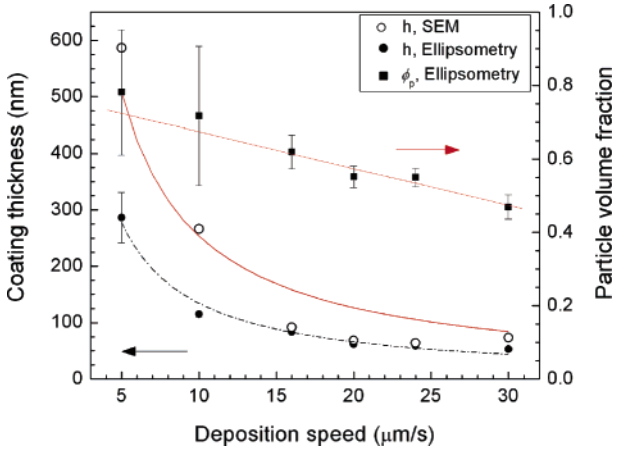


**Figure 3.** Comparison data from ellipsometric and SEM measurements of coating film thickness on silicon substrates. The thickness data are fitted to the expected $\alpha v_w^{-1}$ dependency, where $\alpha$ is a fitting parameter. The particle volume fraction fitted to the effective media model for ellipsometry is plotted on the right-hand axis.

The particle volume fraction in the coatings extracted from the ellipsometry measurements increased with increasing coating thickness (Figure 3). This trend was anticipated

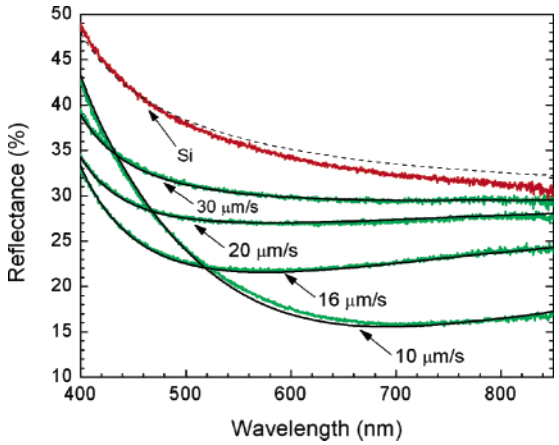


**Figure 4.** Measured and calculated normal incidence reflectance spectra for bare silicon wafer and for Si surface coated with silica at various deposition speeds. Calculations shown as smooth black lines (solid for the coatings, dotted for bare substrate) are overlaying the measured spectra shown in gray. Model curves are fitted to the data by varying $\phi_p$ and $l$.

because the packing efficiency improves as particle films transition from a 2-D system to 3-D system.[32,34] The relative error in the measurements of $\phi_p$ and $l$ at low deposition speeds was large (Figure 3), indicating a comparatively poor fit to the ellipsometric model of uniform layers. Additionally there is a deviation between the results from SEM measurements and ellipsometric measurements at low $v_w$ (below 16 $\mu$m/s). When the film thickness approaches the wavelength of the ellipsometer, interference and scattering may contribute to the error.

The silicon substrates do not transmit light in the UV/visible range, so only reflectance data were gathered from these samples. The coatings visibly reduced the reflectance of the substrate. In Figure 4, varying degrees of AR behavior for different silica coatings on silicon wafer chips are shown and compared with the reflectance of a bare wafer (with a native oxide layer). Qualitatively, the reflectance spectra for various deposition speeds were the same, but the minimum in reflectance shifted to shorter wavelengths for faster deposition speeds. Coatings deposited at 16 $\mu$m/s were more antireflective in the range of 400−500 nm, while coatings deposited at 10 $\mu$m/s were most antireflective in the range of 500−800 nm. These measurements correlate well with the visually observed tint of the coatings, which tended to be blue-green for faster speeds (in agreement with the recorded spectra), but shifted to a yellowish tint for deposition speeds below 16 $\mu$m/s.[38] The shift in reflectance spectra that occurred between deposition speeds 16 and 10 $\mu$m/s can be attributed to a change in film thickness or in refractive index or more likely a combination of both since they are linked to each other.[34] The greatest reduction in reflectance, 51% AR, occurred near 600 nm for the 10 $\mu$m/s coatings, where $R$ decreased from an absolute reflectance of ~30% to ~15%.

Silicon has a complex refractive index with wavelength-dependent real and imaginary components in the visible range,[39] so the Fresnel coefficient in eq 2 changes accordingly.[40] The dotted line in Figure 4 shows the theoretically calculated reflectance of the bare silicon surface (with native oxide layer). The smooth curves overlaying the actual reflectance data for coatings deposited at different deposition speeds are the result of calculations using eq 2, incorporating the known refractive index of the Si substrate,[39] and the effective refractive index from eq 4. The parameters, $l$ and $\phi_p$ in eq 2, were fitted by least-squares error method to match the predicted spectra to the experimental data. The agreement between reflectance data and model is quite good (Figure 4). The relative trends in the values for $l$ and $\phi_p$ obtained from fitting match well the ellipsometry data. In most cases, the values for the reflectance data and the ellipsometry data match within experimental error.

In summary, the SEM, reflectance and ellipsometry data were all mutually supportive, showing that we can control the coating thickness and volume fraction via the meniscus withdrawal rate. The results for coating thickness showed a definite $1/v_w$ trend, corroborating eq 1. Coatings composed of silica particles alone without any additives or substrate modifications reduced the reflectance of silicon by up to 51%. The spectra of the coatings were well modeled by eq 2, showing that the homogeneous film assumption holds well as long as the particles are smaller than the spectroscopic wavelength. By virtue of the deposition process, a desired range of the spectrum could be preferentially absorbed by the silicon substrate. These results could be important for photovoltaic applications of silicon like solar cells, where quantum efficiency must be maximized, and for photodetectors, where signal-to-noise ratios must be as high as possible.

*Glass Substrates.* The silica nanoparticle coatings deposited via convectively assembly onto glass were transparent; i.e., no scattering or opacity was observed due to the small constituent particle size. Visually, the silica nanocoatings were also less reflective than their respective bare glass substrates. Changes in deposition speed resulted in changes in the coloration of the light reflected off the coating, ranging from a blue tint to a yellowish tint as the deposition speed, $v_w$, decreased. The hue of the coatings correlated well with the actual spectra recorded for the individual coatings (Figure 5). In particular, the transmission maxima for the deposition speeds shown in Figure 5b ranged from 450 to 650 nm, which roughly corresponds to the blue, green, and yellow color sequence. The yellowish appearance is partly attributed to the higher reflectance in the 600 nm range, while the bluish tint is attributed to the higher reflectance for the 400−500 wavelengths relative to the reflectance minima near 600 nm.[38]

The transmission spectra for coatings on glass had a sinusoidal shape with a single maximum if the quarter-wave thickness occurred over the range of 400−850 nm (Figure 5). This behavior is typical and expected of single layer coatings (e.g., eq 2). Nonoptimal coatings exhibited minima over this "visible" wavelength range (Figure 5a), because they were either too thick or too thin in comparison to the desired quarter-wave thickness (see, e.g., data for 10 and 40

(38) Kuehni, R. G. *Color: an introduction to practice and principles*; John Wiley and Sons: New York, 1997.
(39) Palik, E. D., Ed. *Handbook of optical constants of solids*; Academic Press: San Diego, CA, 1998.
(40) Stephens, D. J. In *Physics*; North Carolina State University: Raleigh, NC, 1996; p 150.

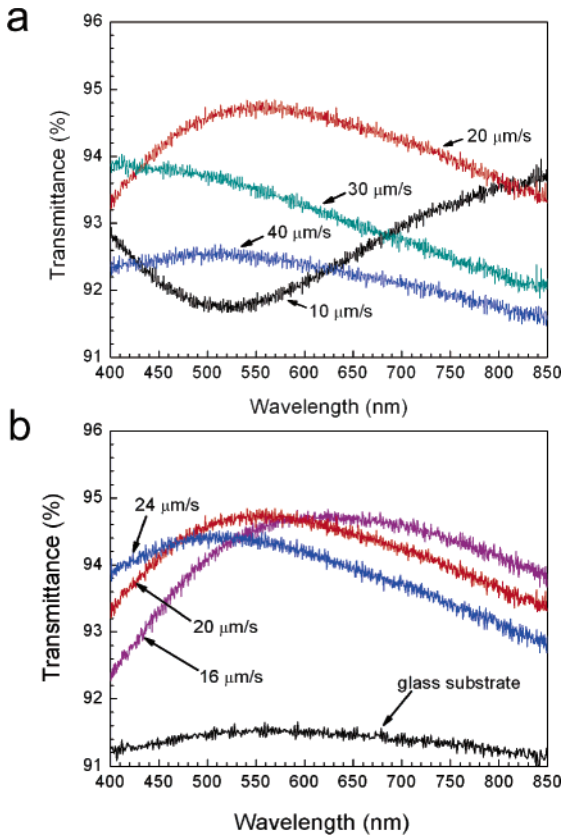


**Figure 5.** Transmission spectra for silica nanocoatings on glass substrates: (a) comparison of broad range of deposition speeds; (b) spectra from the optimal range of deposition speeds. Note the precise control of the maximal AR wavelength via the parameters of the deposition process.

$\mu$m/s, respectively). The maximum obtainable, and reproducible, transmission for a single-sided coating on glass was 94.5−94.8% (Figure 5), which corresponds to ∼70% AR for a single side of glass. The optimal range of deposition speeds for these coatings was centered about ∼20 $\mu$m/s (Figure 5b). Data were collected for deposition speeds of 16, 18, 20, 22, and 24 $\mu$m/s and showed precise tuning of the spectral maxima (for clarity, only three spectra are displayed). The relative difference in spectral behavior for different $v_w$ is caused primarily by varying film thicknesses, $l$, and to a lesser extent by the refractive indexes, $n_c$, both of which are controlled by the deposition speed. The blue shift in the transmission maxima correlates well with increasing deposition speed, proving that the optical properties of the coatings can be controllably varied by the deposition process (Figure 5b).

The structure of the silica nanocoatings on glass was characterized by SEM and profilometry to directly measure the coating thickness, $l$, and to evaluate the packing fraction of the silica spheres (determining AR efficiency through $n_{eff}$). The film thickness data obtained from profilometry for coatings deposited at various deposition speeds are shown in Figure 6. The profilometry data closely matched the thicknesses calculated by fitting the UV/vis transmittance spectra using eq 2, assuming negligible absorption. The fitting protocol was similar to that used for the silicon substrates. The single side calculation was adjusted for the uncoated substrate backside reflectance by subtracting the experimentally measured reflectance loss from a single side

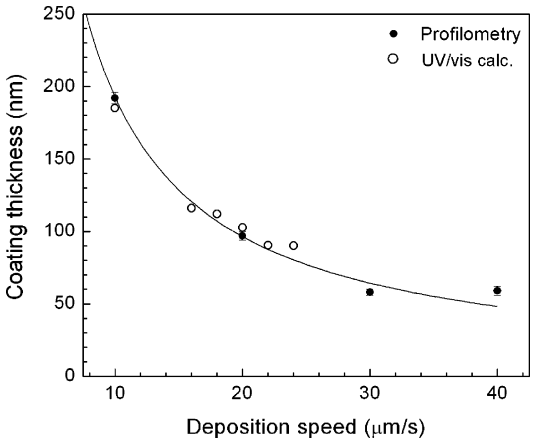


**Figure 6.** Comparison of coating thicknesses on glass measured via profilometry and obtained by fitting UV/vis spectrophotometry data to eq 2. The curve is a fit to the expected $\alpha v_w^{-1}$ dependency.

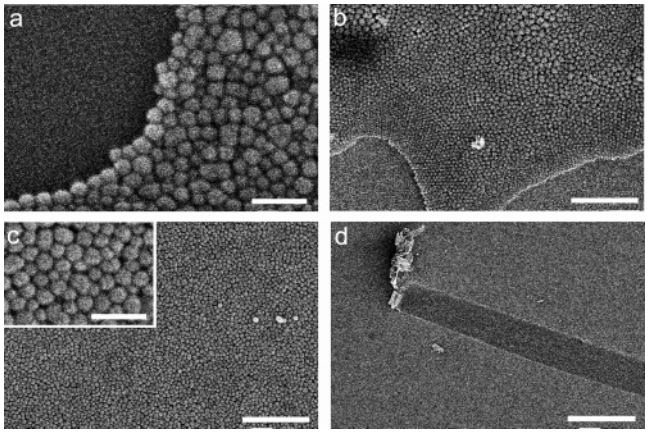


**Figure 7.** Top-down SEM micrographs of silica nanocoating deposited at (a) 22 $\mu$m/s (scale = 200 nm) and (b) 24 $\mu$m/s (scale = 1 $\mu$m), (c) multilayer coating deposited at 16 $\mu$m/s (scale = 1 $\mu$m, inset scale = 200 nm), and (d) low-magnification image of the same coating showing a scratch made during sample preparation (scale = 100 $\mu$m).

for a glass slide over the range of 400−850 nm.[15] Both the UV/vis and profilometry data showed nearly identical $v_w^{-1}$ dependencies (Figure 6), supporting our previous findings on colloidal deposition via convective assembly.[31,32]

In Figure 6, both sets of data approached an asymptotic thickness of ∼65 nm for high deposition speeds—the transition from monolayer to submonolayer formation. At higher speeds the films become submonolayers, with increasing amounts of void space between regions of locally high packing fractions (∼0.65), even though profilometry consistently measured film thicknesses that coincided with the diameter of the silica nanoparticles. Beyond a certain deposition speed, the voids become so large that the homogeneous film assumption fails.

A few coatings deposited at various speeds were investigated using cross-sectional SEM. These were highly charging samples, yielding relatively poor images, but still exhibited increasing film thickness with decreasing deposition speed. The structure of the silica coatings on glass was similar to the ones on silicon. The top-down SEM micrographs show that, for monolayer or thicker, the packing fraction remained relatively uniform, consisting of random close-packed (rcp) spheres (Figure 7). The only deviation in the film structure occurred for coatings deposited at high

deposition speeds (Figure 7a,b), where voids several hundred square nanometers or larger were observed because the deposition speed was too rapid to sustain a continuous film. Such two-dimensional "foam" structures have been reported earlier[32,33,41] and are the result of multiple dewetting events in the drying liquid film. The onset of submonolayer formation at deposition speeds greater than 24 $\mu$m/s correlates to the observed decrease in antireflective efficiency at high deposition speeds (Figure 5a). If the void size approaches or exceeds the wavelength of incident light, the regions of exposed substrate will increase the compound reflectance and cause scattering losses as well. Conversely, if the film is too thick compared to the quarter-wave thickness, the coating AR efficiency is also diminished (Figures 1 and 5b).

The polydispersity of the $SiO_2$ particles resulted in rcp packing with little long range ordering (Figure 7, $\phi_p \sim 0.65-0.75$). Size selective segregation between larger and smaller particles occurred in some localized areas (Figure 7b). Microphase separation of particles with different sizes in dispersed systems has been reported before;[42] however, for convective assembly in thin evaporating films, size selective segregation is considered an artifact from the large particles permitting the small particles to flow in and surround them.[43,44] While long-range crystallinity is essential for self-assembled photonic crystals, long-range order in colloidal silica particle films is not required for AR.[27] The small size (74 nm) of the particles used in this study makes their ordering irrelevant. However, while the coatings are not crystalline, the low magnification SEM images in Figure 7c,d demonstrate consistent long-range uniformity of the coating thickness, which is essential for this application.

The data analysis shows that the silica coatings deposited between 16 and 20 $\mu$m/s are of the proper quarter-wavelength film thickness for AR in the visible region. However, UV/vis transmittance data show that the coatings eliminate only 3% of a possible 4.3% reflectance at a single side, which for two-sided coating translates to ≈98% absolute *T*. These coatings will remain at 1−2% below the theoretical transmission maximum, which occurs at $\phi_p \sim 0.45$ (Figure 1). This trend can be seen more clearly in Figure 8a, where we have plotted calculated reflectance data, assuming a quarter-wave thickness for the coating. There are two possible volume fractions that could cause a reflectance of ∼1%, but our investigation of the coating microstructure proved that $\phi_p$ is centered around ∼0.7; hence $n_c \sim 1.34$ (Figure 8a). Further confirmation is shown in Figure 8b, where calculated spectra for silica coatings of 112 nm thickness overlay the actual spectra of a silica nanocoating (deposited at 18 $\mu$m/s). Using eq 2 as a function of wavelength, for $l = 112$ nm, $\phi_p = 0.745$ provided the best fit of the calculated spectra to the data. For the same coating thickness ($l = 112$ nm), complete AR at a wavelength of 555 nm is predicted for $\phi_p = 0.45$ (Figures 1 and 8). Thus, the factor limiting the AR efficiency of these particle coatings is not the thickness but the coating porosity which dictates the effective refractive index. The analysis of the data demonstrates that a lower $\phi_p$ is required to attain 100% *T*.

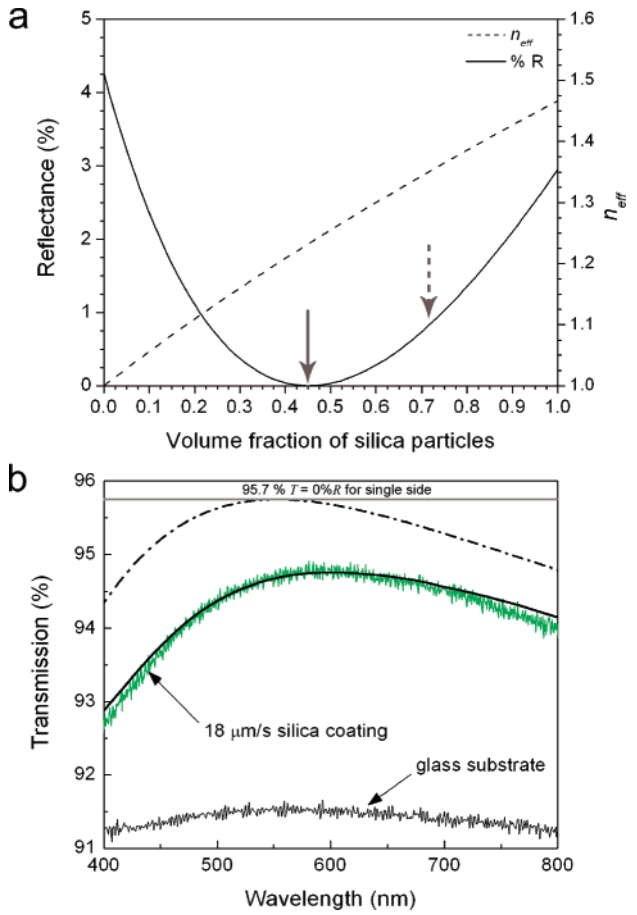


**Figure 8.** (a) Reflectance calculation for single-side quarter-wave thickness silica coating on glass using eq 3. The effective refractive index of the coating from eq 4 is plotted on the right axis for reference. The dotted arrow shows the position of the typical experimental reflectance measured in terms of the coating volume fraction. The solid arrow shows the optimal $\phi_p = 0.45$ for maximal antireflectance. (b) Comparison of best single-side experimental spectra and spectra calculated using eq 2 fitted with $\phi = 0.745$ and $l = 112$ nm (—). For reference, the optimum *T* for $\phi = 0.45$ and $l = 112$ nm is shown (- − -).

In summary, using the same controlled deposition procedures for glass and silicon substrates, $SiO_2$ nanocoatings provided up to 70% and 51% relative reduction in reflectance losses, respectively. Multiple characterization techniques, supported by modeling, show that the coatings on both substrates are very similar in structure and properties. The film thicknesses measured or fitted follow closely the expected inverse dependence on deposition speed. The convective deposition driving forces far outweigh any electrostatic and van der Waals contributions,[45] and the coating thickness can easily be tuned to the desired range. The packing fraction in these coatings assembled from a single type of silica particles, however, was higher than the optimal one for 100% suppression of reflectance. To increase the AR efficiency, we investigated in the second part of this work a few strategies for deposition of films of increased porosity.

(41) Kralchevsky, P. A.; Denkov, N. D. *Curr. Opin. Colloid Interface Sci.* **2001**, *6*, 383−401.
(42) Hachisu, S.; Kose, A.; Kobayashi, Y.; Takano, K. *J. Colloid Interface Sci.* **1976**, *55*, 499−509.
(43) Lazarov, G. S.; Denkov, N. D.; Velev, O. D.; Kralchevsky, P. A.; Nagayama, K. *J. Chem. Soc., Faraday Trans.* **1994**, *90*, 2077−2083.
(44) Yamaki, M.; Higo, J.; Nagayama, K. *Langmuir* **1995**, *11*, 2975−2978.
(45) Israelachvilli, J. *Intermolecular and surface forces*, 2nd ed.; Elsevier Science Ltd.: London, 1992.

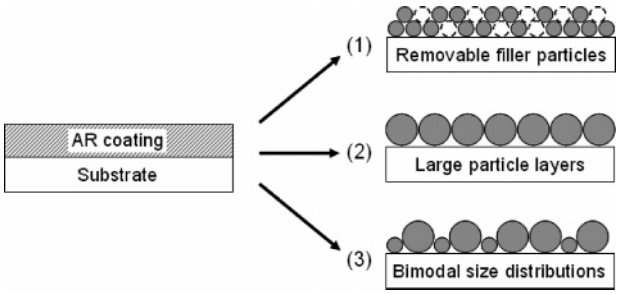


**Figure 9.** Schematic of the three experimental strategies used to increase the porosity of the silica coating structure and thus reduce their effective refractive index.

**Controlling Coating Porosity.** The above analysis shows that silica coatings made from single-sized particles are limited to relatively high volume fractions ($\phi_p > 0.65$) due to the close packing of the constituent particles. Three different strategies were tried to increase the coating porosity and decrease the refractive index while maintaining consistent quarter-wave coating thicknesses (Figure 9). First, the use of removable organic filler particles was tested using mixed-particle coatings comprised of silica and polystyrene (PS) deposited from binary suspensions (both ~70 nm diameter). Second, larger silica particles of 134 nm were used to lower the refractive index while maintaining the thickness near the average quarter-wave thickness for the visible region. Last, binary mixtures of the large and small silica particles were used to break up the close-packed structure of the coatings, while maintaining the desired quarter-wave thickness.

**Removable Organic Filler Particles**. Evenly distributed organic particles such as PS microspheres could reduce the coating porosity after the sacrificial PS spheres were removed using either calcination (pyrolytic etching)[46] or dissolution. Since coatings from single-sized particles were limited to filling fractions of approximately 70% (Figure 8a), and the target fraction was 45% for maximal AR, mixtures of 2:1 and 3:1 silica/polystyrene by volume were made (both particles ~70 nm). The hypothesis was that the PS particles would randomly distribute throughout a silica particle matrix, yielding a coating that had the same ratio of silica to PS as the original binary mixture. Additionally, the small size of the PS particles would ensure that void space generated by their removal would be subwavelength and well distributed. Similar procedures have been used before to create more porous colloidal crystals by LBL deposition of silica and then PS microspheres,[46] by controlled chemical etching of the existing hcp silica microsphere array[47] and by back-filling a silica sol matrix around an existing sacrificial PS colloidal crystal template to make inverse opals.[48−50]

Prior to removing the PS, the transmittance spectra of mixed PS/silica coatings were very similar to the silica coatings seen earlier, but they were on average slightly lower, having average starting point of approximately 93.5−94% (maximum) transmittance. This was attributed to the relatively high refractive index of the PS component ($n = 1.59$). The results after applying both techniques of PS latex sphere removal were inconsistent and inconclusive. Small improvements in the transmission were observed; the best improvement was 95% absolute $T$ (~75% decrease in reflectance for one side). However, in many cases, after PS removal the transmission did not change or even decreased below 93.5%. Additionally, after etching, there was often a significant shift in the spectral profile, indicating a microstructural change that could be attributed to collapse of the coating structure due to capillary forces for wet etching or sintering and fusion of the silica particles during the pyrolytic etching. One cause for this poor reproducibility could be that the polystyrene is microphase segregating into polystyrene-rich domains (for more details see the Supporting Information).

**Varying Particle Size**. The packing efficiency of a particle coating increases with the number of particle layers, and thus, monolayers have the lowest packing fraction. Coatings from monodisperse, larger particles with diameters equal to the quarter-wave thickness (134 nm) would have $\phi_p = 0.605$. If these larger particles could be deposited in a submonolayer coating with uniform small voids, $\phi_p$ would be reduced further still, potentially approaching the target 0.45. The deposition of such coatings proved elusive, mainly because the transition from monolayer to submonolayer is difficult to control microscopically due to capillary immersion forces. Thus, the spectra for a uniform monolayer of larger particles were approximately the same as for the multilayer small particle coatings, with a maximum of 94.5−94.8% $T$ (Figure 10a). The transmission increased slightly with increasing deposition speed, maxing out at 95% $T$. Beyond that critical point the transmission dropped very quickly, nearly back to the glass background (8.6% $R$), which we attribute to the large size of the voids occurring in the submonolayer structure. In practice, the reduction of $\phi_p$ by using only a single layer of particles (Figure 11a) does not give much better results than multilayer coatings of small particles.

**Binary Mixtures of Different Sized Particles**. Thin coatings from mixtures containing particles of two mean sizes were deposited with the goal of disrupting the close-packed structure and decreasing the packing efficiency in the coatings. If two types of particles are deposited in a layer by layer fashion (large particles first, then smaller ones), the smaller particles fill space selectively around larger particles, forming a binary crystal structure that depends on $\gamma$, the ratio of the small to large particle radii.[46,51] In simultaneous single-step deposition by convective assembly the particles can still pack into binary crystals, but long-range ordering becomes less favored as $\gamma$ exceeds 0.22 due to electrostatic and entropic effects.[51,52] If the particles are slightly polydisperse as the ones used in this study, jamming and mutual disruption of array formation are likely to occur.

For this series of experiments, aqueous binary sols with $\gamma \sim 0.55$ were prepared by mixing together 74 and 134 nm

(46) Velikov, K. P.; Christova, C. G.; Dullens, R. P. A.; van Blaaderen, A. *Science* **2002**, *296*, 106−109.
(47) Fenollosa, R.; Meseguer, F. *Adv. Mater.* **2003**, *15*, 1282−1285.
(48) Velev, O. D.; Kaler, E. W. *Adv. Mater.* **2000**, *12*, 531−534.
(49) Vlasov, Y. A.; Astratov, V. N.; Karimov, O. Z.; Kaplyanskii, A. A. *Phys. Rev. B* **1997**, *55*, 357−360.
(50) Velev, O. D.; Tessier, P. M.; Lenhoff, A. M.; Kaler, E. W. *Nature* **1999**, *401*, 548−548.
(51) Wang, D. Y.; Mohwald, H. *Adv. Mater.* **2004**, *16*, 244−247.
(52) Kitaev, V.; Ozin, G. A. *Adv. Mater.* **2003**, *15*, 75−78.

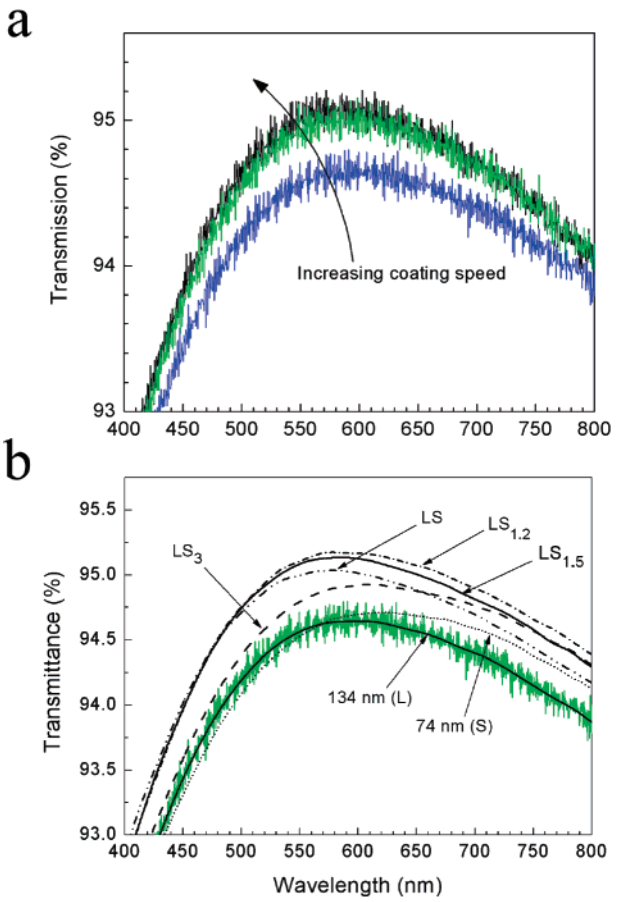


**Figure 10.** (a) Transmission spectra for 130 nm $SiO_2$ coatings deposited at speeds between 10 and 20 $\mu$m/s. (b) Transmission spectra for coatings made from a mixture of large (average diameter 134 nm) and small (average diameter 74 nm) particles in different ratios. The stoichiometric ratio of particles in the mixed particle coatings is given as $LS_n$.

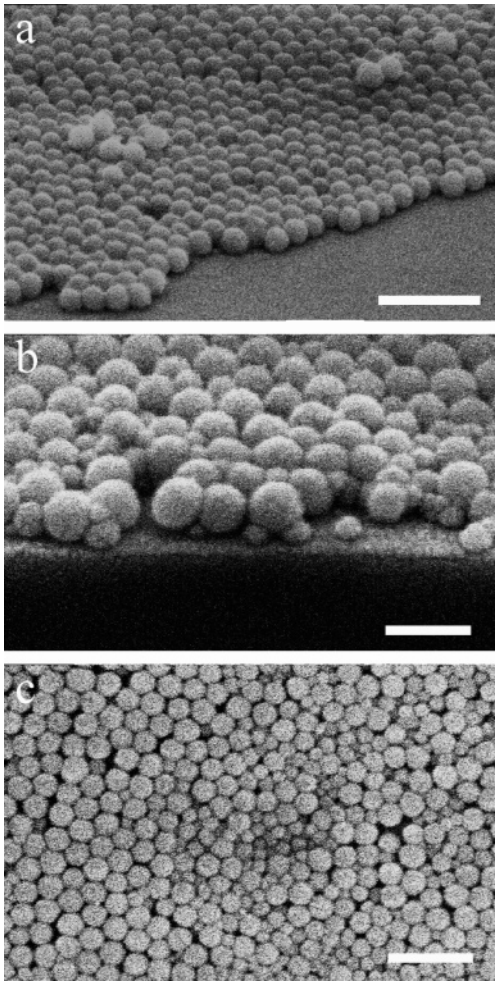


**Figure 11.** (a) Cross-sectional SEM of 130 nm $SiO_2$ sphere monolayer (scale = 1 $\mu$m), (b) cross-sectional SEM of a $LS_{1.5}$ mixture of 130 and 70 nm $SiO_2$ particles (scale = 200 nm), and (c) top-down image of the same $LS_{1.5}$ coating (scale = 400 nm).

$SiO_2$ suspensions. We sought to deposit only a single layer with all particles lying on the substrate, in which case the small ones would disrupt the close-packing of the larger particles while maintaining an effective film thickness equivalent to the large particle diameter (thus increasing the porosity). When the deposition conditions are optimized, a single layer coating of distributed large particles locally surrounded by smaller particles can be obtained. Figure 10b shows a comparison of spectra from coatings of small particles, large particles, and mixed large/small particle coatings. For viewing convenience, the raw spectral data have been smoothed, which also serves to more clearly show the average transmission maximum. It is clear that the best AR coatings (with largest porosity) were formed from mixtures of large (L) to small (S) particles in stoichiometric ratios of $LS_{1.5}$ and $LS_{1.2}$. The maximal absolute transmittance achieved with one coated side was 95.2% $T$ (or effectively 0.5% $R$/side) at a wavelength of 575 nm. From eq 2, the best fit of the $LS_{1.2}$ spectra was $l = 113.5$ nm and $\phi_p = 0.665$. This coating had the highest transmittance and lowest volume fraction in all experiments.

Coatings composed of either $LS_{1.2}$ or $LS_{1.5}$ particle ratios could potentially have localized regions of LS and/or $LS_2$ lattice crystals. For $\gamma = 0.55$, the calculated particle filling fractions in a binary lattice hcp monolayer (with all particles lying on the basal plane) are 0.49 for an $LS_2$ structure and 0.43 for an LS arrangement. Thus, by geometric arguments, the LS ratios yielding the best AR results ($LS_{1.2}$ and $LS_{1.5}$) were in the correct range to theoretically attain the optimal packing fraction (0.45). SEM showed that while the addition of small particles in these ratios did serve to break up the large particle monolayer into a more randomized structure, binary crystallization was not observed (Figure 11b,c). Locally, there were regions with some ordering, and there were also local cases of size selective segregation as well (Figure 11b,c). Other researchers have reported random arrangement in coatings from binary systems when $\gamma > 0.3$.[52]

The disrupted microstructure and low packing fraction of these binary mixture coatings made them the most effective AR materials obtained in this study. A demonstration of the efficacy of these AR coatings is shown in Figure 12. An uncoated glass slide was compared to a glass slide coated on each side with a $LS_{1.5}$ mixture of the large and small $SiO_2$ nanoparticles. The image under the uncoated glass is completely obscured by the very bright specular reflection. The image below the coated plate can clearly be seen because the coatings on both sides are antireflective and transparent. Consequently, single-step convective assembly of binary mixture of 134 and 74 nm particles reliably reduced the absolute reflectance for a singled-sided glass from 4.3% to an average 1.4% over the 400−850 nm range (with a minimum of 0.5% $R$ at 575 nm). This reflectance reduction

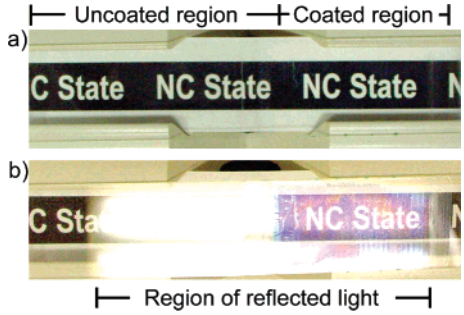


**Figure 12.** Demonstration of good antireflective coating on a glass microscope slide (both sides coated, right) compared to an uncoated plate (left): (a) top-down image (ambient lighting) showing transparency of coating; (b) same sample, under conditions of strong specular reflectance. Reflected light photo was taken with strong light source approximately 20° off normal and camera approximately −20° off normal.

translates to an AR efficiency of 67% on average over this spectrum and a maximal efficiency of 88% at 575 nm. The use of coatings from nanoparticle mixtures appears to be an effective means to make improved antireflective coatings. Notably, this improved performance is achieved without making the method more complex or costly.

One additional parameter employed in characterizing the optical properties of AR films is hazing, which historically has been used to describe polymer thin films.[53] Domains of different density within semicrystalline polymer films may cause scattering that lead to losses in direct transmission through a sample. Hazing is defined as the fraction of light transmitted through a sample that deviates (by forward scattering) from the beam axis by more than 2.5°.[53] A specific transmission detector is required to perform this test (ASTM 1003);[53] however, one can estimate the losses from off-axial scattering by analysis of the reflected and directly transmitted light data. The angle of spatial collection of our spectrometer in transmission mode is less than 2.5°, so the light lost due to hazing is subtracted from the direct transmission data. The average sum of the complimentary reflectance and transmittance data for our single-layer coatings (either from single particles or mixed particles) yielded $R + T = 99.67 \pm 0.12\%$. Thus, on average ≈0.3% was lost due to scattering (or hazing). This is not a large amount of scattering, which explains why the coatings appear visibly clear (Figure 12). For the spectral range studied, the losses due to hazing were greatest in the near UV/blue region as expected from the theory of scattering from small particles. The small size of the particles and the lack of larger-scale domains limit the losses due to hazing in our coatings.

These coatings adhere relatively well to the substrate and require some effort to be scratched off by metallic stylus (cf. Figure 7d). The relatively good adhesion and cohesion, compared to other types of nanoparticle coatings,[31] is likely a result of the similar chemical nature of the particles and substrates, which maximizes van der Waals attraction. Improvement of the adhesion and stability of these coatings is an issue that is currently being investigated. Brief sintering of the coating should improve coating cohesion and adhesion without appreciably decreasing the AR capabilities.

(53) Wang, L.; Kamal, M. R.; Rey, A. D. *Polym. Eng. Sci.* **2001**, *41*, 358−372.

Single-layer coatings as the one described here are limited to a single maximum transmission wavelength. The performance of our coatings is comparable to commercial single layer antireflective coatings while deposited in a much more rapid and inexpensive technique. Commercial (vacuum-deposited) multilayer "stack" coatings of high and low refractive index materials use multiple interference, which yields a broad spectral range of suppressed reflectance. The AR performance of such multilayer graded optical coatings would be superior to ours, but the potential advantage of this method would be in making large-scale inexpensive coatings rather than coatings with exceptional optical quality. Further optimization of the coatings and scaling up of the technique appear feasible and straightforward.

## Conclusions

In this report, we show that convective nanoparticle assembly can provide an efficient economic alternative to AR coating deposition by conventional techniques. The AR coatings were deposited in a single step from microliter droplets of aqueous colloidal silica dispersions. No pretreatment of the particles or the substrate was required. The control over film thickness afforded by the deposition technique allowed the reflectance/surface to be reduced by up to 51% and by up to 70%, respectively, for Si wafers and for glass. The limiting factor with this deposition technique turned out to be the silica volume fraction in the coatings. We demonstrated that this restriction can be overcome simply by mixing silica particles of different sizes, which mutually disrupt their structure to yield more porous coatings with lower refractive index. By using binary mixtures of large and small $SiO_2$ nanoparticles, the coating reflectance was further reduced to yield up to an 88% AR efficiency. The process may be optimized further by judicious selection of deposition conditions, particle sizes, and particle refractive indexes to provide a nearly complete AR band over a large portion of the spectrum. The main advantages of the process are the use of inexpensive commercial silica suspensions without any chemical additives, organic solvents, or vacuum technologies. The low cost, scalability, and simplicity of the technique could make possible applications for which the present methods are too expensive, such as routine large-scale deposition of coatings on surfaces of windows and solar cells.

**Acknowledgment.** This material is based upon work supported in part by the STC Program of the National Science Foundation under Agreement No. CHE-9876674, the Army Research Office, and by the Department of Chemical and Biomolecular Engineering at NCSU. Y.H. greatly appreciates the support provided by the LG Yonam Foundation during his stay at NCSU as a visiting scientist. The authors thank Olivier Cayre of the University of Hull for the particle size measurements, the Genzer group at NCSU for the use of their VASE ellipsometer, and the Parsons group at NCSU for the use of their profilometer.

**Supporting Information Available:** Examples of microscale phase separation in coatings of mixed silica and latex spheres. This material is available free of charge via the Internet at http://pubs.acs.org.

CM050416H